AIAA 2004-2247

Instability and Transition in the Mach-6 Quiet Tunnel

Steven P. Schneider, Shann Rufer, Craig Skoch, Erick Swanson, and Matthew P. Borg

School of Aeronautics and Astronautics
Purdue University
West Lafayette, IN 47907-1282 USA

34th Fluid Dynamics Conference

28 June - 1 July 2004

Portland, OR

Instability and Transition in the Mach-6 Quiet Tunnel

Steven P. Schneider*, Shann Rufer†, Craig Skoch‡, Erick Swanson§, and Matthew P. Borg¶
School of Aeronautics and Astronautics
Purdue University
West Lafayette, IN 47907-1282

Abstract

Laminar-turbulent transition is critical for vehicles which fly significant distances at hypersonic speeds. To improve on existing correlations, prediction methods that incorporate knowledge of the transition mechanisms are necessary and now feasible. Purdue continues to develop the Boeing/AFOSR Mach-6 Tunnel to seek quiet flow at high Reynolds number, with noise levels comparable to flight. Measurements of the fluctuations in the contraction entrance are reported, along with measurements of the effects of disturbances introduced downstream. Progress towards conventional-noise measurements at high unit Reynolds number is also described, along with preliminary hot-wire measurements on a cone at angle of attack.

Introduction

Hypersonic Laminar-Turbulent Transition

Laminar-turbulent transition in hypersonic boundary layers is important for prediction and control of heat transfer, skin friction, and other boundary layer properties. Vehicles that spend extended periods at hypersonic speeds may be critically affected by the uncertainties in transition prediction, depending on their Reynolds numbers. For example, the HCV and CAV vehicles being designed under the DARPA FALCON program will probably require laminar-flow control to be successful [1]. However, the mechanisms leading to transition are still poorly understood, even in low-noise environments.

Many transition experiments have been carried out in conventional ground-testing facilities over the past 50 years [2]. However, these experiments are contaminated by the high levels of noise that radiate from the turbulent boundary layers normally present on the wind tunnel walls [3]. These noise levels, typically 0.5-1% of the mean, are an order of magnitude larger than those observed in flight [4, 5], and can cause transition to occur an order of magnitude earlier than in flight [3, 5]. In addition, the mechanisms of transition operational in small-disturbance environments can be changed or bypassed altogether in high-noise environments; these changes in the mechanisms change the parametric trends in transition [4]. Mechanism-based prediction methods must be developed, supported in part with measurements of the mechanisms in quiet wind tunnels.

Development of Quiet-Flow Wind Tunnels

Only in the last two decades have low-noise supersonic wind tunnels been developed [3, 6]. This development has been difficult, since the test-section wall boundary-layers must be kept laminar in order to avoid high levels of eddy-Mach-wave acoustic radiation from the normally-present turbulent boundary layers. A Mach 3.5 tunnel was the first to be successfully developed at NASA Langley [7]. Langley then developed a Mach 6 quiet nozzle, which was used as a starting point for the new Purdue nozzle [8]. Unfortunately, this nozzle was removed from service due to a space conflict. The new Purdue Mach-6 quiet flow Ludwieg tube may become the only operational hypersonic quiet tunnel in the world.

Background of the Boeing/AFOSR Mach-6 Quiet Tunnel

A Mach-4 Ludwieg tube was developed at Purdue in 1992-1994 [9]. Quiet flow was achieved at

*Professor. Associate Fellow, AIAA.
†Research Assistant. Student Member, AIAA.
‡Research Assistant. Student Member, AIAA.
§Research Assistant. Student Member, AIAA.
¶Research Assistant. Student Member, AIAA.

low Reynolds numbers, and the facility was used for development of instrumentation and for measurements of instability waves under quiet-flow conditions. However, the low quiet Reynolds number and the small 4-inch test section imposed severe limitations.

A low-cost hypersonic facility that remains quiet to higher Reynolds numbers is needed. Beginning with Ref. [10], a series of AIAA papers have reported on the design, fabrication, and shakedown of this facility, on the development of instrumentation, and on progress towards achieving Mach-6 quiet flow at high Reynolds number.

Ref. [11] summarized these earlier papers, reported on initial quiet flow achieved at low Reynolds numbers with the 6th bleed-slot design, and also on initial measurements with temperature-sensitive paints and hot wires. Ref. [12] reported temperature-sensitive-paints results on the forebody, the results of the 7th bleed-slot throat geometry, and the (minimal) effect of polishing the downstream portion of the Mach-6 nozzle. Ref. [13] reported initial measurements of bypass transition on the nozzle wall, the apparent elimination of low-pressure separation after removing the double-wedge model-support centerbody, and high levels of static-pressure fluctuations in the diffuser when the nozzle-wall boundary layer is laminar, as well as hot-wire and temperature-paints measurements on a sharp cone. Ref. [14] reported more measurements of bypass transition on the nozzle wall, along with the disappointingly minor effect of bypassing the bleed-slot air direct to the vacuum tanks. It also reported more measurements in the diffuser, the first measurements in the contraction entrance, initial measurements of condensation, the successful fabrication of a new sting support, and preliminary hot-wire measurements on cones, along with hot-wire calibrations.

The present paper reports progress in the first half of 2004. Efforts to achieve quiet flow at high Reynolds number presently fall into three categories: 1) measurements in the contraction entrance, seeking noise sources in the flow entering the throat, 2) measurements downstream of the nozzle, seeking evidence regarding the possible upstream propagation of downstream noise sources, and 3) computations of the flow in the bleed slot, seeking evidence of fluctuations that can trip the flow downstream. Recent computations show that a separation bubble is forming on the main-flow side of the bleed lip [15]; at present, this appears to be the most likely cause of early transition. However, the other approaches continue to be studied in parallel. In addition, the tunnel and instrumentation continue to be developed for conventional-noise operation at high unit Reynolds number, to enable study of transition caused by crossflow and roughness. Finally, progress with hot-wire measurements on cones is reported.

The Boeing/AFOSR Mach-6 Quiet Tunnel

Quiet facilities require low levels of noise in the inviscid flow entering the nozzle through the throat, and laminar boundary layers on the nozzle walls. To reach these low noise levels, conventional blow-down facilities must be extensively modified. Requirements include a 1 micron particle filter, a highly polished nozzle with bleed slots for the contraction-wall boundary layer, and a large settling chamber with screens and sintered-mesh plates for noise-reduction [3]. To reach these low noise levels in an affordable way, the Purdue facility has been designed as a Ludwieg tube [9]. A Ludwieg tube is a long pipe with a converging-diverging nozzle on the end, from which flow exits into the nozzle, test section, and second throat (Fig. 1). A diaphragm is placed downstream of the test section. When the diaphragm bursts, an expansion wave travels upstream through the test section into the driver tube, and a fast valve is opened to initiate flow in the bleed slots. Since the flow remains quiet after the wave reflects from the contraction, sufficient vacuum can extend the useful runtime to many cycles of expansion-wave reflection, during which the pressure drops quasi-statically.

Fig. 2 shows the last section of the nozzle. Here, z is an axial coordinate whose origin is at the nozzle throat. The region of useful quiet flow lies between the characteristics marking the onset of uniform flow, and the characteristics marking the upstream boundary of acoustic radiation from the onset of turbulence in the nozzle-wall boundary layer. A 7.5-deg. sharp cone is also drawn on the figure. The rectangles are drawn on the nozzle at the location of window openings, all but one of which are presently filled with blank metal inserts. Images of the tunnel are available at `http://roger.ecn.purdue.edu/~aae519/BAM6QT-Mach-6-tunnel/`, along with earlier papers and other documentation.

Pre-Run Free Convection in the Contraction Entrance

One of the sources of early transition on the nozzle walls could be fluctuations in the flow entering the nozzle throat. Although considerable care was taken

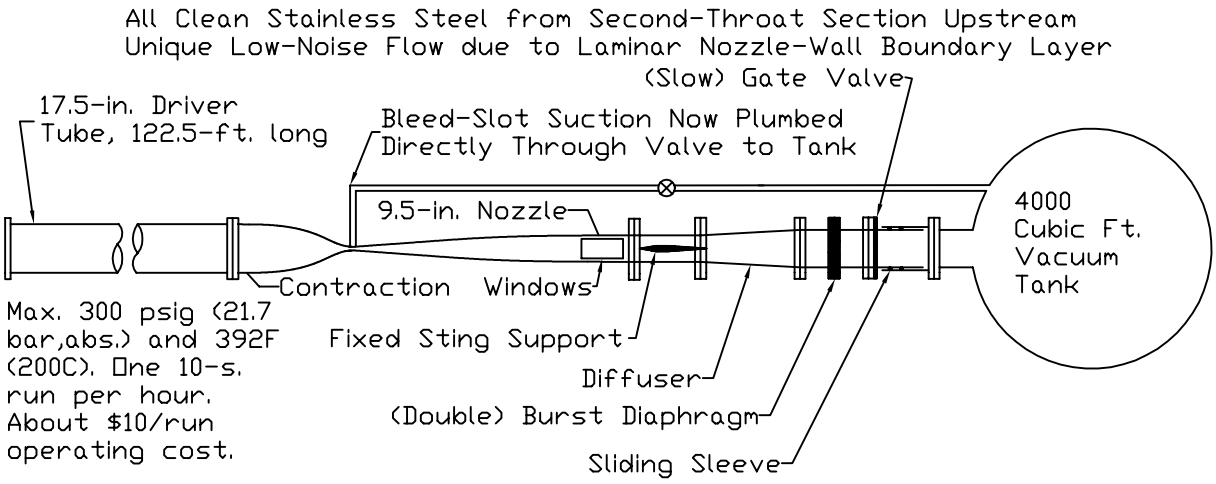

Figure 1: Schematic of Boeing/AFOSR Mach-6 Quiet Tunnel

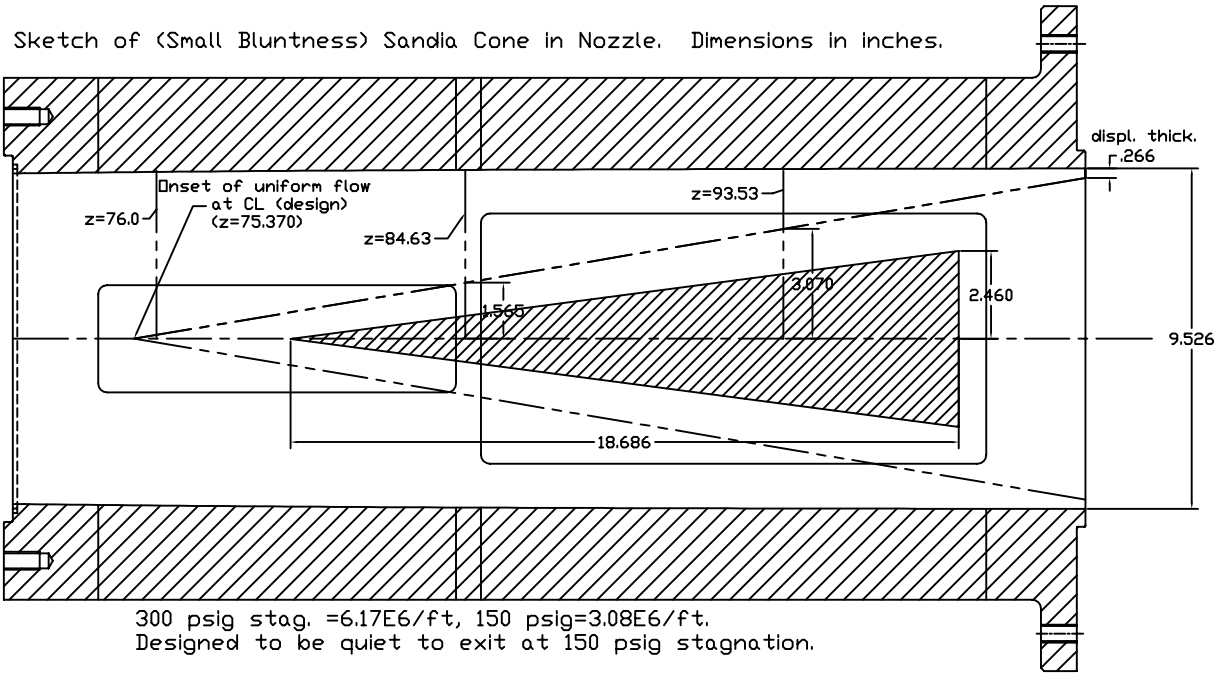

Figure 2: Schematic of Mach-6 Quiet Nozzle with Model

to obtain clean, dry, stagnant air of uniform temperature in the driver tube and contraction, nonuniformities may still exist. To investigate this possibility, it is desirable to make measurements in the driver tube and contraction. This is not easy, since both are ASME code-stamped pressure vessels, and not readily modified. However, measurements are possible using two access ports provided at the entrance to the contraction, near the driver tube exit. The access ports are centered 6.500 inches downstream of the beginning of the contraction, where the tunnel radius has decreased only to 8.705 inches, from 8.750 inches in the driver tube [14].

One of the possibilities for generating noise is free convection in the nominally stagnant driver tube air, prior to the beginning of the run. If free convection exists and sets up significant nonuniformities in the air, they could convect downstream once flow has begun, and cause early transition. Previous hot-wire measurements showed a significant level of seemingly random fluctuations in the flow leaving the contraction [14], and later measurements showed significant hot-wire voltage fluctuations before flow was initiated. It was thus necessary to determine if the pre-run fluctuations were due to free convection in the contraction, free convection due to the difference in temperature between the heated hot wire and the cooler tunnel air, or fluctuations due to a generally nonuniform tunnel temperature.

Previously, these random fluctuations were recorded at a hot wire location $y = -0.94$ in. down from the top contraction wall, at driver tube pressures of approximately 25 psia and 100 psia. At that time, the contraction temperature was much lower than the rest of the driver tube, since the contraction-wall heaters were turned off to ease access into the contraction. This access difficulty was overcome by removing the 1-in.-dia. upper instrument port when inserting hot wires, rather than opening the joint between the first and second portions of the contraction. The hot wire was successfully inserted into the fully heated contraction ($160°C$) using this new method.

For all measurements taken, the standard bridge on a TSI IFA100 constant temperature anemometer (CTA) was used in conjunction with an 8-bit Tektronix TDS7104 digital oscilloscope. With the tunnel heated, the best hot-wire overheat ratio that could be obtained was at first only 1.09; here the wire was tuned to obtain the maximum frequency response. In this state, the hot wire was on the verge of being unstable and thus was very susceptible to oscillations. Thus, the operating resistance

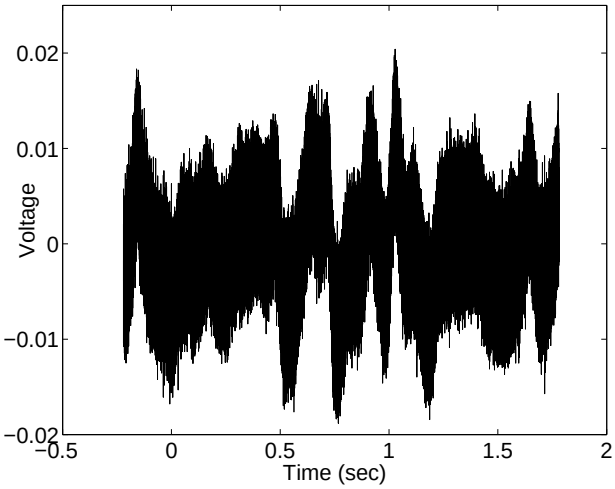

Figure 3: Hot-wire trace for hot contraction after 80 min. for $P_d = 25$ psia and $y = -0.94$ in.

could not be adjusted any higher without causing the hot wire output to oscillate. It is thought that the low overheat ratio obtained was because the cold temperature of the wire was already $160°C$ due to tunnel heating. In order to obtain a better overheat ratio, the hot wire was slightly detuned. This meant that the hot wire was much more stable, and an overheat ratio of 1.52 was achieved. The hot wire has not yet been calibrated; the method to be used is yet to be determined, for these low-Mach number flows with varying mean density.

Previously, the first time the low frequency fluctuations were recorded, they were seen most markedly at a driver tube pressure of 25 psia. Thus, a driver tube pressure of $P_d = 25$ psia was selected. The hot wire was lowered to a position $y = -0.94$ in. from the upper contraction wall. Nineteen hot-wire voltage traces were then recorded over a period of approximately 24 hours. Fig. 3 shows a trace taken at 80 minutes, with an overheat ratio of 1.52. Fig. 4 shows a CTA output trace from a previous experiment, with an overheat ratio of 1.64. The only difference in setup, besides the different overheat ratios, is that Fig. 3 was obtained with the contraction fully heated to $160°C$, while Fig. 4 was recorded while the contraction was unheated.

It was surprising to see higher fluctuations in the fully heated contraction than in the cooled contraction, despite the somewhat lower overheat ratio. When the contraction was cooled, the rest of the tunnel was still heated to approximately $100°C$. This resulted in a large temperature gradient over the contraction section. It was thought that this large

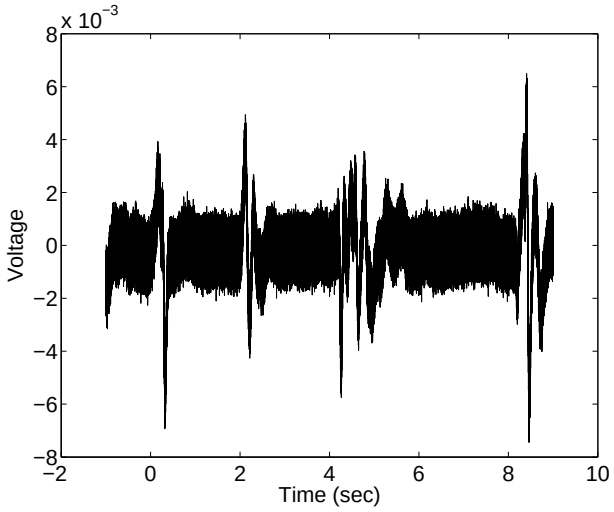

Figure 4: Hot-wire trace with cold contraction after about 25 min., for $P_d = 25$ psia and $y = -0.94$ in.

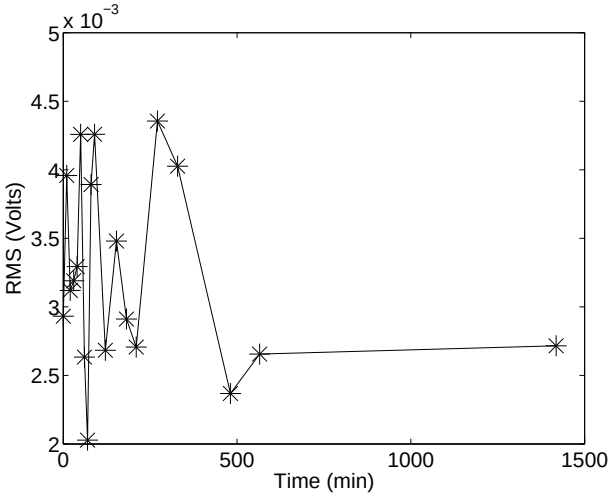

Figure 5: RMS voltage on hot wire for $P_d = 25$ psia and $y = -0.94$ in.

temperature gradient was responsible for inducing free convection in the contraction section, and thus the large intermittent fluctuations observed in Fig. 4.

It was thought that keeping the tunnel and contraction section heated uniformly to approximately $160°C$ would remove the tunnel temperature nonuniformity, and thus remove or lessen free convection within the contraction section. This would, in turn, produce smaller fluctuations in the CTA output signal. However, this was not the case. Instead, the fluctuations with a uniform tunnel temperature were about a factor of 4 larger than those recorded for a cooled contraction. This might be attributed to the fact that the downstream section of the contraction near the 1-inch nozzle throat was not heated. Since the tunnel was heated to $160°C$, not $100°C$ as in Fig. 4, an even larger temperature gradient existed near the end of the contraction. It would be good to make similar measurements upstream, towards the center of the driver tube, to avoid contraction-end temperature gradient effects, but the code-stamped driver tube has no access ports to enable such measurements. A new pipe section with instrumentation ports would have to be built and inserted between the flanges of the existing pipe to enable such measurements.

Fig. 5 shows the RMS voltage fluctuations for the hot contraction case. Each point corresponds to the RMS calculated from an entire oscilloscope record: 10 seconds for the first 8 points, and 2 seconds for subsequent points. Sampling frequencies were 250 KHz for the first 7 points, 125 KHz for the 8th point, and 1 MHz for subsequent points. The scope record lengths and sampling frequencies were changed in an attempt to further improve oscilloscope resolution. The electrical RMS noise was subtracted from the signal by measuring the RMS at vacuum (roughly 50 torr) and computing the square root of the difference of the squares of the signal RMS and the vacuum RMS. It cannot be assumed that the RMS voltage levels out after approximately 500 minutes, as there were not enough readings taken past 500 minutes to validate such a claim. It should be noted that after 61 minutes, the oscilloscope was changed from standard to Hi-Res mode to improve signal resolution. In Hi-Res mode, data is sampled at 1GHz and averaged into memory at the set sampling rate.

The hot wire was then moved to a position near the centerline, -9.0 in. from the top contraction wall, and similar measurements were recorded, again with the hot contraction. Fig. 6 shows a trace recorded approximately 1 minute after the tunnel was pressurized. Fig. 7 shows the corresponding RMS (minus the electrical RMS measured at 47 torr) vs. time. Each point corresponds to the RMS calculated from an entire scope record of 2 seconds with a sampling frequency of 1 MHz.

Note that the RMS fluctuation levels near the centerline are typically less than half of those observed at the same pressure but $y = -0.94$ in. from the top contraction wall. A visible comparison between Figs. 3 and 6 shows a sharp contrast: Fig. 6 has a much steadier signal.

During the time between recordings, the nature

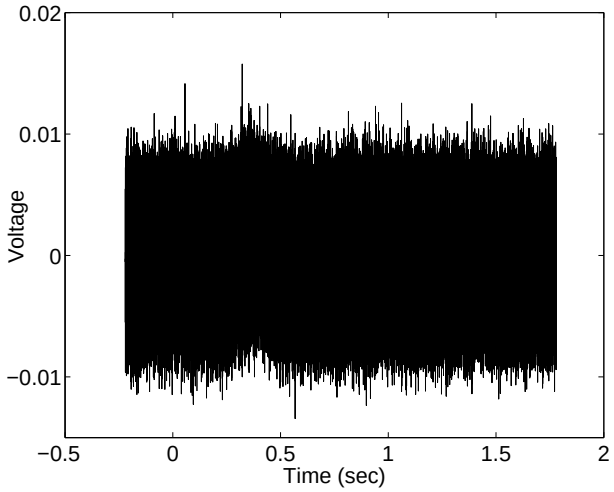

Figure 6: Hot-wire trace after 1 min. for $P_d = 25$ psia and $y = -9.0$ in.

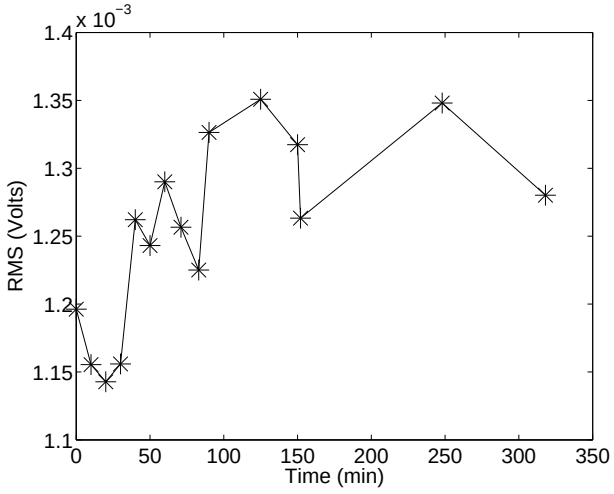

Figure 7: RMS voltage for $P_d = 25$ psia and $y = -9.0$ in.

of the hot-wire output for either location did not vary much. At $y = -0.94$ in., the low frequency fluctuations continued, but did not change observably in amplitude or frequency. At $y = -9.0$ in., there were occasional small fluctuations, as can be seen in Fig. 6 near 0.4 seconds. The amplitude and frequency of these disturbances did not vary much over time.

Further experimentation was done so as to ascertain how far from the upper contraction wall free convection effects extend, as well as how free convection affects tunnel operations. A driver tube pressure of 26 psia was chosen because previous measurements of free convection were conducted near this pressure.

In this case, an overheat ratio of 1.62 was used for all data recorded. The tunnel temperature was set to 160°C. All oscilloscope traces were recorded with a sampling frequency of 500 kS/s.

The tunnel was pressurized to approximately 26 psia. Immediately after the tunnel pressure had equilibrated, an oscilloscope trace of the CTA output was recorded. Oscilloscope traces were then recorded every 10 minutes over a period of 2 hours for hot wires located -.10, -.35, -.60, -1.10, and -1.35 in. down from the top wall. Traces were also recorded for 80 minutes at a hot-wire location of -.85 in. Additionally, traces were recorded over a 30 minute period for hot wires located -1.50, -2.00, -2.50, -3.00, -3.50, -4.00, -4.50, -5.00, -5.50, -6.00, and -6.50 in. down from the top wall. Later records were taken over a shorter time period as no significant difference could be seen between oscilloscope records taken after 30 minutes and records taken after 120 minutes. As before, an additional trace was recorded at near vacuum (~ 1.7 psia) in order to subtract background electrical RMS fluctuations from traces recorded at pressure.

Figs. 8, 9, and 10 are typical oscilloscope traces for wires positioned at three locations. As can be seen in these figures, as well as Fig. 11, the average RMS level (believed to correspond to free convection) was smaller closer to the wall, then increased to its maximum value at around -1.5 in, and then decreased to its minimum value. Electrical RMS was subtracted from the CTA signal by computing the square root of the difference of the squares of signal RMS and vacuum RMS. In Fig. 11, for all wall distances, the first half hour of the scope records were averaged.

This behavior was not expected. It was thought that if a wall effect were causing the observed free convection, the effects would be greatest near the

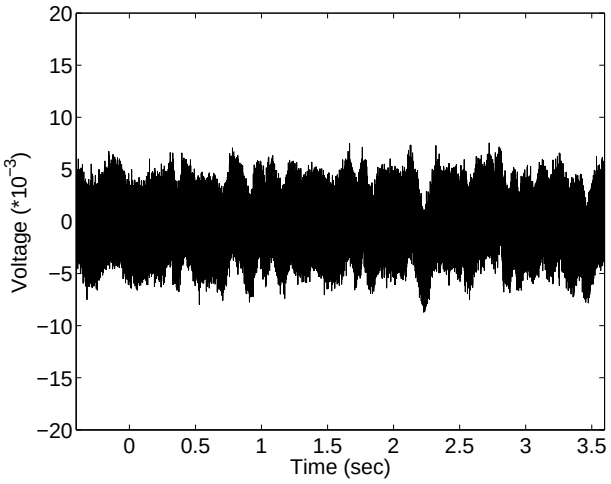

Figure 8: Sample oscilloscope trace at $y = -.10$ in after 30 minutes

wall and then decrease as distance from the wall increased. This is clearly not the case; rather, some sort of free-convection boundary-layer seems to be forming. Before any conclusions can be drawn, however, these results must be checked for repeatability.

At distances of -.10 in and -3.00 in, Figs. 8 and 9, a number of large-scale fluctuations can be seen. These are believed to be caused by free convection. At -6.00 in, Fig. 10, the number of such fluctuations is greatly reduced. This is in keeping with previous measurements that demonstrated a higher level of free convection fluctuations closer to the wall, and fluctuations at a much diminished level closer to the tunnel centerline.

Hot-wire measurements were also made during tunnel runs in order to see what effect, if any, free convection had on tunnel runs. Runs were made with the hot-wire located -.50, -1.00, -1.50, -2.00, -2.50, -3.00, -3.50, -4.00, -4.50, -5.00, -5.50, -6.00, and -6.50 in. down from the top contraction wall. Fig. 12 shows the RMS vs. distance from the upper contraction wall. For all the runs, the stagnation pressure was about 26 psia, the stagnation temperature was about $140°C$, and the RMS was calculated using one of the quasi-steady periods between expansion waves, approximately 160 ms after tunnel startup. As can be seen, the RMS during runs was an order of magnitude larger than RMS calculated for quiescent fluid. This may be due only to the higher mean heat transfer during the run; calibrated measurements are needed to determine the meaning of the amplitudes. The cause for extraneous point at y=-6.50 in is unknown. There is nothing in the data to suggest that such a steep change in RMS should

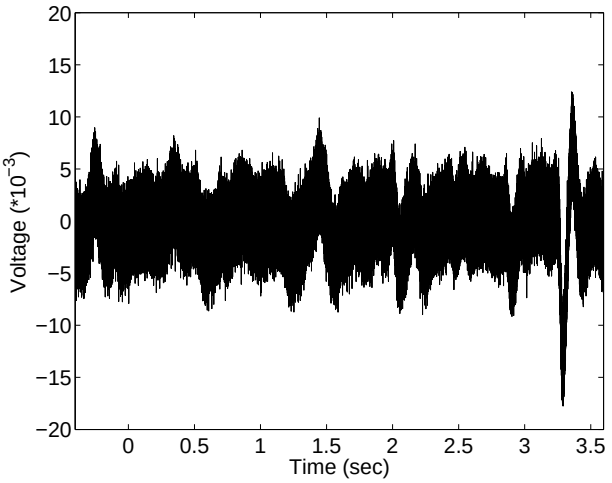

Figure 9: Sample oscilloscope trace at $y = -3.00$ in after 30 minutes

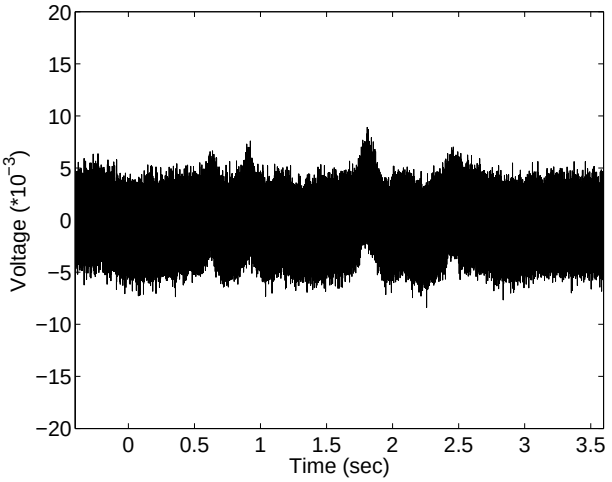

Figure 10: Sample oscilloscope trace at $y = -6.00$ in after 30 minutes

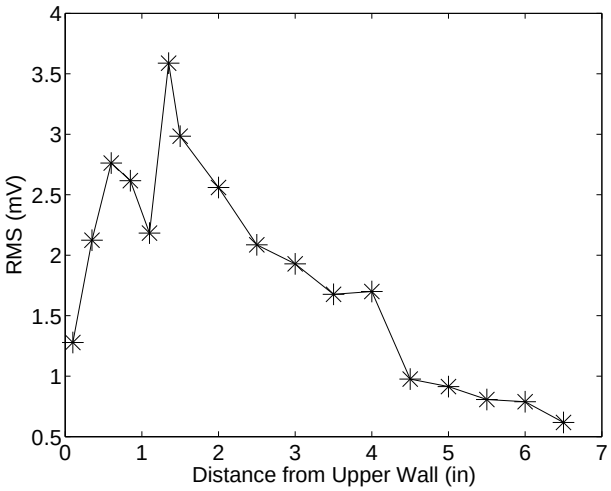

Figure 11: Average RMS vs. Distance from Wall, quiescent fluid

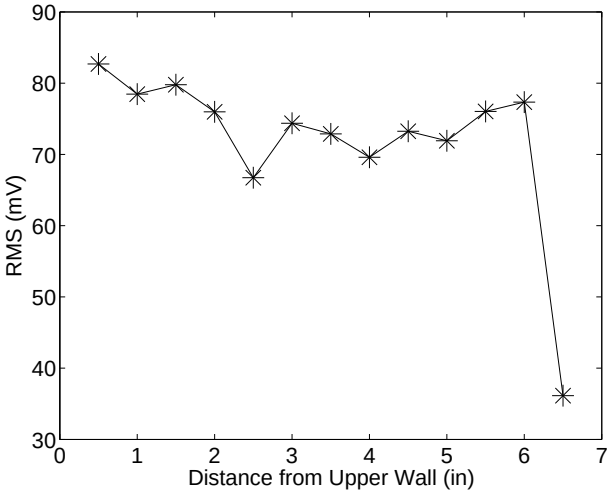

Figure 12: RMS vs. distance from upper contraction wall for tunnel runs

occur at this point. Since no points were taken at hot-wire locations farther from the upper contraction wall, this point should be disregarded until it can be checked for repeatability.

Fig. 13 shows a typical power spectra obtained from data recorded for a hot wire in quiescent fluid. The three peaks at approximately 52.75 kHz, 59.50 kHz, and 105.25 kHz are present in nearly all oscilloscope traces recorded for quiescent fluid. Similar spikes at frequencies of 52.75 kHz and 105.25 kHz were observed in the power spectra for almost all runs and can be seen in Fig. 14.The cause of these spikes is unknown at this time, but electrical interference is suspected.

The additional spikes in Fig. 14 between 11 and 16 kHz are also present in the power spectra for several other runs. In a number of other runs, as can be seen in Fig. 15, there is a much larger spike at 12.00 kHz. The cause for these spikes, and the discrepancy in the spectra between 11 and 16 kHz in Figs. 14 and 15 is also unknown at this time.

Although more measurements are needed, the data suggest that free convection in the contraction is primarily limited to fluctuations near the wall, and that free convection from the heated wire to a nominally uniform flow has a negligible effect. More measurements will be taken to ascertain the repeatability of current data, to explain the aforementioned discrepancies, and to quantify the amplitude of the fluctuations.

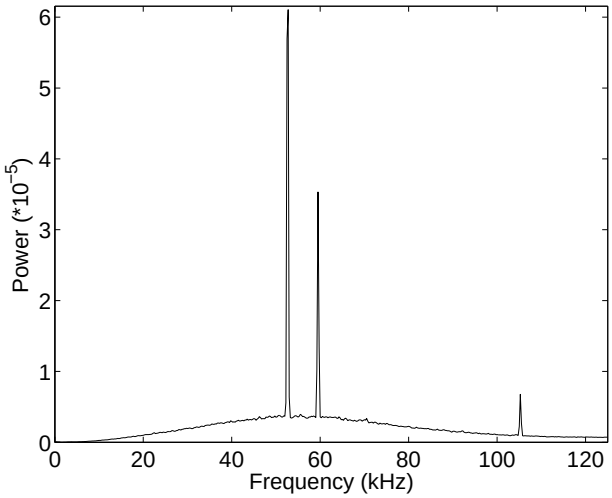

Figure 13: Power spectrum for quiescent fluid, $y = -4.00$ in. The highest peaks are at 52.75 kHz, 59.50 kHz, and 105.25 kHz

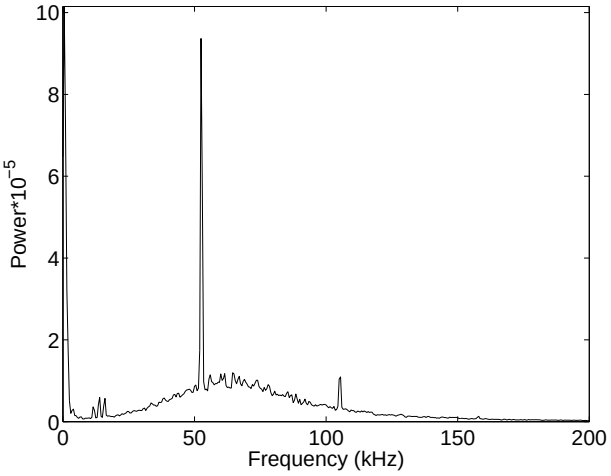

Figure 14: Power spectrum for run, $y = -4.00$ in.

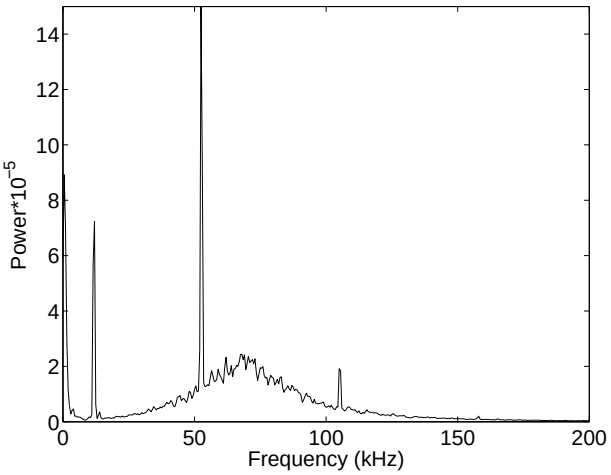

Figure 15: Power spectrum for run, $y = -5.00$ in.

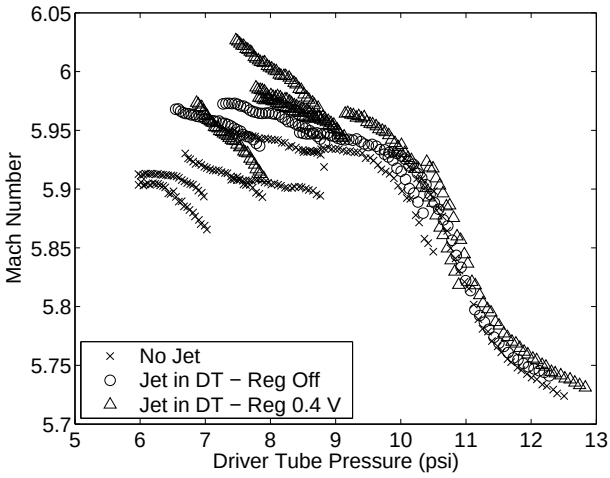

Figure 16: Mach number with jet in driver tube

Effect of Introducing Disturbances in the Driver Tube

To approach the upstream noise issue from the other direction, experiments were performed to see what level of disturbances is necessary to disrupt quiet flow. This knowledge could help determine what prevents quiet flow at higher pressures. The disturbance in the driver tube was introduced through the pipe at the far upstream end of the driver tube that supplies the air to the tunnel. A jet was introduced by blowing air through the supply pipe, with the pressure regulator set to 0 volts and to 0.4 volts. The shutoff valve that normally prevents air from entering during a run was left open for these tests. When the pressure regulator is set to 0 volts, it attempts to keep the pressure at 1 atm; when the driver tube is below 1 atm, air will be leaked in. The leak rate associated with this varies from about 0.016 kg/s at a driver pressure of 8.5 psia to 0.004 kg/s at a driver pressure of 10 psia. This leak rate will continue to decrease to zero as 1 atm is approached. When the pressure regulator is set to 0.4 volts, the pressure behind the regulator is approximately 10 psig. This results in a mass flow rate of about 0.06 kg/s for driver-tube pressures of 8-14 psia.

Fig. 16 shows the Mach number that was measured over 0.1-sec intervals during runs with the jets in the driver tube and with no jet. The pitot Kulite was on the centerline at $z = 75.3$ in., the driver-tube temperature was $160°C$ and the dewpoint was not measured since the driver tube was below ambient pressure so the air does not readily flow past the dewpoint meter. The Kulite was not corrected for

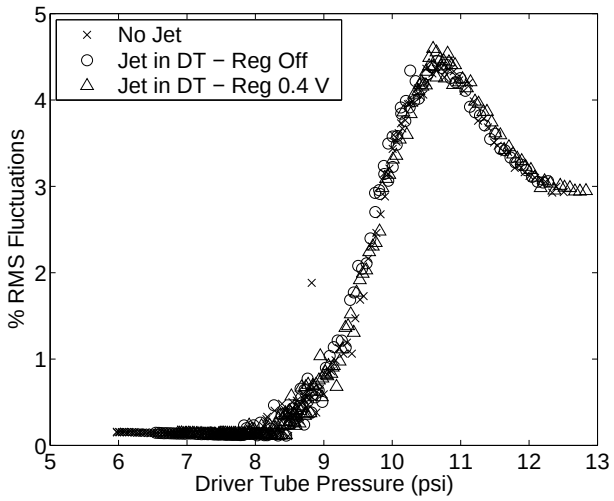

Figure 17: RMS fluctuations with jet in driver tube

temperature effects. The Mach number appears to be slightly lower for the case with no jet, but the difference is not large compared to the scatter in the data. The Mach number increases as the pressure falls, possibly because the nozzle-wall boundary layer is becoming more laminar and therefore thinner.

The initial driver tube pressure for each run was not controlled as precisely as it usually was, since the jet had to be started before the run started, and the time for the diaphragm burst can vary by up to 30 seconds. For the case with no jet, the initial driver tube pressures were 7.98, 7.99, 9.00, 9.99, 10.00, 12.00, and 14.34 psia. For the case with the jet (valve open), but with the regulator off, the initial driver tube pressures were 8.08, 9.00, 10.13, 11.94, and 14.10 psia. For the case with the jet, and with the pressure regulator set to 0.4 volts, the initial driver tube pressures were 8.40, 9.50, 9.86, 10.07, 12.18, and 14.56 psia.

Fig. 17 shows the percent RMS pitot fluctuations on the nozzle centerline for the same runs. This shows the noise dropping out at about the same driver tube pressure for all cases. This data shows that these weak jets introduced in the upstream end of the driver tube had no effect on the pressures at which quiet flow could be achieved.

Leak Tests

It is well known in the quiet tunnel community (e.g., Jim Kendall and Steve Wilkinson, private communications) that leaks in the low-pressure sections of a quiet tunnel can trip the laminar boundary layer and preclude quiet flow. Leaks in these regions (settling chamber, contraction, and nozzle) would be expected to generate jets of air flowing from outside the tunnel into the low-static-pressure tunnel air; these cause disturbances in the freestream and are also likely to trip the boundary layer. For example, Jim Kendall recalls that a missing half-inch bolt in the 8 or 10-ft dia. settling chamber of the JPL 20-inch supersonic tunnel (which ran quiet at low Reynolds numbers [16, 17]) would cause a substantial leak that would preclude quiet flow; also, leaks in the seals at the corners of the rectangular nozzle would also preclude quiet flow (private communication, June 2004). Thus, leak tests are necessary to ensure there are no small leaks that might preclude quiet flow. Although the tunnel had been previously tested by pressurizing it, spraying on a soap-film solution, and looking for air bubbles, a more sensitive leak test seemed desirable.

Pressure-Drop Measurements

Initial leak tests were performed by filling the tunnel to about 150 psia and seeing how quickly the air leaks out of the tunnel. There is some error in this method as the pressure appears to be highly sensitive to the temperature of the tunnel. The slight fluctuations that occur when the power supplies heating the driver tube turn on and off can give increases and decreases in pressure of about 0.1%, even while the temperature is at equilibrium. This is significant since the leak rate in some cases is less than this per hour. This variation could be accounted for if the mean temperature of the air was known, but there is only one thermocouple for the air, at the far upstream end of the driver tube, and this thermocouple does not accurately show what is happening in the rest of the tunnel. This temperature-induced error was minimized by waiting until the pressure drop due to air leaks was significantly larger than the variation due to temperature effects. In most cases this required running the leak test for 15 to 20 hours and applying a linear fit. Although the pressure in a tank with a sonic orifice actually drops exponentially, a linear fit was instead used for convenience. In cases with a larger leak rate, the variation due to temperature fluctuations is not as important since the leak rate is comparatively large.

An equivalent orifice size was also calculated to estimate the overall size of the gaps in the tunnel causing the leaks. This was done by using the pressure drop and the volume of the tunnel to find the mass flow of air leaving the tunnel. An assumption of isentropic flow to a sonic throat was made, and

the area of the throat was used as the estimate of the area of the cumulative gap size.

It has been noted in the past that the flanges on the driver tube leak after they have been heated and cooled a few times. The silicone O-rings do not maintain a reliable seal, despite their $450°F$ rating and the $392°F$ maximum temperature used; instead, they rapidly take a compression set after a few months, and then leak when the tube is cooled. A leak test with the driver tube cold and the flanges in the driver tube leaking showed a leak rate of 18% in one hour and an equivalent orifice of 2.01 sq. mm. Without changing the O-rings, the driver tube was heated and the leak test was repeated to give a leak rate of 0.07% per hour over 14 hours and an equivalent orifice of 0.0048 sq. mm. This indicates that the O-rings expand and fill the gap when heated, even after they have taken a permanent compression and do not seal when cold. The heated leak rate is small enough that it seems unlikely to affect quiet flow.

The driver tube was heated again to stop the leaks in the driver tube, in order to perform a helium leak test (which will be described shortly). Two leak tests with the helium gave leak rates of 0.30% and 0.36% per hour over 20 hours and 29 hours, respectively, from initial pressures of 140 and 151 psia. The equivalent orifice sizes were 0.0065 and 0.0085 sq. mm. This is a higher leak rate than with air, which may be the result of the smaller ratio of specific heats for helium. Another leak test was performed with air while a window blank replaced the plexiglas window. This gave a leak rate of 0.04% per hour over 16 hours and an equivalent orifice of 0.0035 sq. mm. It was noticed that the O-ring on the window was somewhat frayed, which could explain the leak. However, after the window O-ring was replaced with a new O-ring, another test with air gave a leak rate of 0.17% per hour over 14 hours and an equivalent orifice of 0.0115 sq. mm. This is even higher than the previous leak test with the window in place, which could indicate the window is leaking again. The driver tube was not cooled between these tests, so a new leak in the driver tube is unlikely.

Helium-Sniffer Measurements

A leak test was then performed using a precision helium sniffer. The leak detector was a Model 21-250 GOW-MAC gas leak detector, manufactured by GOW-MAC Instrument Co., which operates by measuring the thermal conductivity of the gas being sampled and comparing it to that of air. It is quoted as being able to easily detect helium leaks as small as 10^{-5} cm^3/s. In operation it is somewhat slow to respond. Leaks generally seem to take about 90 seconds to register, so when an area was checked, the probe was left in place for at least 2 minutes to give any leak time to register. Some of this delay is probably due to the slow rate at which air is drawn into the instrument. The leak detector has a graduated analog scale from -50 to 50. A deflection of 10 corresponds to a leak rate of about 10^{-5} cm^3/s of helium when on the high sensitivity setting. The smallest leak detected resulted in a deflection of about 20, though in most cases, the leaks that were found caused full scale deflections.

The tunnel was pressurized to 151 psi with 99.995% pure helium. Each flange in the nozzle was checked in 8 to 12 places, with fewer places being checked on the smaller flanges. No leaks were detected on any of these flanges. The joints in the contraction were checked in about 6 to 10 places per flange. The only leak detected in the contraction was in the plug on the top instrumentation port. This could not be checked with bubble testing, since it was heated to above boiling. The Swagelok on this plug was tightened, and the leak disappeared. The window blanks in section 8 (the last section of the nozzle) were checked in several places each, with no leaks detected. The seals in the traverse were also checked, with no leaks detected. The window in section 8 was found to be leaking most of the way around it. This was the most widespread leak that was found. This could not be detected with the bubble test since the sealing surface is not visually accessible.

The joints in the diffuser were checked at about 4 to 6 locations per joint and many of the plugs were also checked. There were no leaks discovered in the diffuser except for the connection to the Paroscientific pressure gauge. This leak was also detected through a bubble test. The leak detector found that some helium was leaking past an aluminum plate that replaced the burst diaphragms in the diaphragm section. This could account for some of the leak in the pressure leak tests.

The joints in the driver tube were checked at 5 locations per flange, with no leaks detected. This shows that the O-rings did seal when heated, even when they are known to leak when cold. The end cap at the upstream end of the driver tube was also checked, along with all of the plugs and ports in the cap. No leaks were detected.

Summary of Leak Tests

The helium leak test showed that there are no leaks in the driver tube, contraction, or nozzle that should be preventing quiet flow. The leak in the window is a little troublesome, but it has been shown that a much larger leak is necessary to disturb the flow this far back in the nozzle. Therefore, the remaining small leaks should not be affecting quiet flow.

Initial High Reynolds Number Operations

Motivation

Crossflow and roughness-induced transition are to be studied on blunt-nosed cones at angle of attack [2, 14]. To obtain information on the transition mechanisms, affordable transition data is in many cases desirable. The Boeing/AFOSR Mach-6 Ludwieg Tube is rated for a maximum stagnation pressure of 300 psig, but is presently only operated up to about 130 psig. A boost pump has been added to enable us to reach the higher stagnation pressures, so that conditions for transition on blunt cones can be approached.

Redesigned Gap Plumbing

The plumbing used to control the pressure in the gap between the two diaphragms was redesigned for operation at 300 psig. All piping, pipe fittings, and valves are stainless steel and rated at 1000 psig or better. A 300 psig stainless steel gauge is used to measure gap pressure, and a new stainless steel vacuum gauge was installed for use in low pressure runs. The new plumbing system takes up somewhat less room than the previous design. It has also reduced the leaking problem encountered with the previous system. Initial operation of the new system has gone well, both at the lower Reynolds numbers utilized earlier and in the high Reynolds number tests described below.

Boost Pump

A Corken Industrial D-Style oil-free compressor, Model D-291, has been installed as a boost pump to raise the pressure in the Mach 6 Ludwieg Tube to 300 psig. The single-stage compressor is plumbed into the existing Ludwieg tube plumbing. A bypass valve is closed to protect the upstream air system from overpressurization. The two-piston compressor is mounted in the Boeing Compressible-Flow Machinery Space, along with the Ludwieg tube vacuum pump and the main 50HP compressor that supplies air to the building. Remote 'On' and 'Off' switches are also located on the wind tunnel control panel.

The D-291 has a maximum working pressure of 350 psia, a maximum outlet temperature of $350°F$, and operates up to 15HP. The displacement range is 8.0 cfm at 400 rpm to 16.5 cfm at 825 rpm. The bore is 3.0 in. and the stroke is 2.5 in.

Suction and discharge valves on the inlet and outlet allow air flow into and out of the compression chamber. The valves open when the pressure on one side exceeds that on the other. Thus, when the piston compresses the air on the upstroke, the suction valve closes and the discharge valve opens. The opposite occurs to draw in new air on the downstroke. The discharge valve will close when the pump is turned off, isolating the air in the plumbing and the tunnel from the compressor.

A Barksdale Temperature Switch ML1H-H452S is installed on the exhaust plumbing. The switch monitors the temperature of the exhaust and cuts power to the compressor if it gets too high. A Johnson Controls P70AA-118 low-pressure cut-out switch will be installed on the inlet plumbing to cut power if the inlet pressure drops below about 100 psia. If the inlet pressure drops too low, it can pull oil out of the system. A Johnson Controls P70CA-3C high-pressure cut-out switch will be installed on the outlet plumbing to cut power if the outlet pressure reaches the limit on the tunnel. Ball valves can be used to shut off the inlet and outlet piping. Finally, a 275-psig pop-off valve has been installed on the exhaust to limit the pressure in the tunnel to the maximum permitted by the bleed-slot hoses.

Burst Diaphragm Testing

New diaphragm materials have been tested for operation at higher stagnation pressures. To run under these conditions, the diaphragms must be strong enough to withstand differential pressures up to 150 psi. The strongest diaphragms currently in use burst at around 75 psi.

The diaphragms were tested one at a time. One diaphragm was put in the diaphragm rings (see Ref. [18]) and these were inserted into the tunnel. The gate valve was opened to allow air to flow into the vacuum tank after the diaphragms burst. The driver tube pressure was increased until the diaphragm burst. The pressure in the tunnel at the time of the burst was recorded with a Paroscientific pressure gauge. Each diaphragm material was tested

four times to determine repeatability. The range of break pressures for single diaphragms is shown in Table 1. In preliminary double-diaphragm runs, about 1 in 5 of the 5052 diaphragms broke about 5-10 psi earlier.

Some of the higher-pressure diaphragms began to leak as the pressure was increased. The pressure difference across the diaphragm would deform it into a bowl shape and pull it away from the rings. As this happened, the diaphragm would extrude around the bolt holes. The increased hole area would allow leaking of upstream air into the vacuum tank. The torque on the bolts was increased to prevent this.

Table 1 lists the characteristics of the diaphragms found to be useful at higher pressures. The material, thickness, pressure difference at burst, pressure and Reynolds number range for tunnel runs (when two diaphragms are used in the rings), and the required torque on the bolts are listed for each diaphragm material. New materials are required to extend the range above 250 psia and will be tested in the future. The operating pressure range does not yet extend to $2\Delta p$, since reliable runs become more difficult as the not-yet-broken diaphragms become stressed nearer to their break pressure. Since the maximum cold-wall temperature of the hoses from the bleed slots presently limits operations to 275 psig, and since the 10% increase from 275 psig to 300 psig is of uncertain value, near-term operations will probably be limited to 275 psig.

Initial Operation of Boost Pump

The boost pump currently brings the tunnel pressure up to only 235 psia due to the wiring of the control circuit for the pressure regulator at the driver tube inlet. This wiring is being modified to allow the boost pump to bring the pressure up to 300 psi. The boost pump can be operated from the pump room or from a panel next to the tunnel. The latter is ideal, since the pump can be easily controlled as a run is being made. Under typical conditions, the boost pump increases the driver tube pressure by 0.2 psi/sec.

The pump causes vibrations in the piping carrying the air into the driver tube; these cause vibrations in the tunnel platform. The vibrations are apparently due to the slugs of air that the pump pushes into the pipe. The vibrations may be reduced if the pump is sped up, increasing the frequency of the air slugs and also the fill rate; the original design allowed for this, and this modification will be performed soon.

Initial Tunnel Runs at High Reynolds Number

Several high-pressure runs were made in the Mach 6 Ludwieg Tube, using the boost pump and the new diaphragm materials. The driver tube is filled up in the usual manner until the pressure reaches about 140 psia, which is near the limit on the main compressor. The valves to the boost pump inlet and outlet are opened at the beginning of the day. The valve bypassing the boost pump is manually closed after the driver tube reaches about 140 psia. The boost pump is then turned on using the controls on the panel next to the tunnel. The pressure regulator is immediately turned on and the voltage is set to 5 V. The tunnel is then pressurized up to the desired pressure (up to 230 psia for the current tests). The pressure regulator voltage is increased periodically to maintain a pressure increase of about 0.2 psi/s. This allows air into the tunnel at a rate sufficient to preclude excessive pressure rise at the outlet of the pump, so that the relief valve located at the pump outlet will not reach 275 psig and blow. The boost pump and pressure regulator are turned off from the panel when the desired pressure is reached. The gap pressure is maintained at half the driver tube pressure as usual. At these higher pressures, the gap pressure tends to leak up and must be relieved by slightly opening the downstream valve on the gap plumbing, exhausting some of the air to the vacuum tank. The diaphragms burst cleanly at the expected pressures.

A problem with unexpected pitot probe motion has been encountered. The probe moved from the centerline into the upper-wall boundary layer at some point during the tests, resulting in low pitot pressure measurements and high noise measurements. Large aerodynamic forces might be encountered if the probe is at angle of attack; however, it appears to be parallel to the flow. The probe may be pushed upward during pump-up, since the pressure pushing on the part of the probe inside the tunnel is greater than that pushing on the part of the probe outside the tunnel. The cause of this motion is still being investigated, as is vibration of the 12-inch long pitot during the run.

Despite the problems with probe motion, two good runs were made at the relatively low pressures of 150 psia and 180 psia. The data for these runs are shown in Table 2. The Mach number and noise level are consistent with earlier measurements at lower pressures. A normalized pitot trace at 180 psia is shown in Fig. 18. Here, p_{01} is the stagnation pressure as measured near the contraction inlet, and p_{02} is the pitot pressure in the nozzle. The bleed slots

Aluminum	Thickness	Δp	Torque	p_0 range	Re range
	(inch)	(psi)	(lb.-ft.)	(psia)	($\times 10^6$/ft)
7075	0.025	82-90	95	135 - 160	2.7 - 3.2
5052	0.032	112-116	125	170 - 220	3.4 - 4.4
5052	0.040	131-137	125	225 - 260	4.5 - 5.2

Table 1: Burst Diaphragms for High Pressure Operation

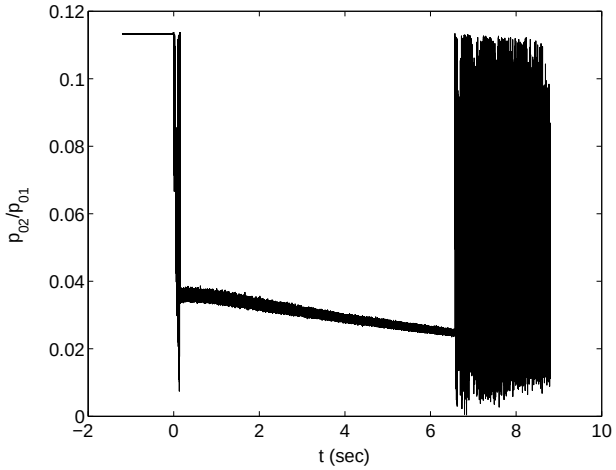

Figure 18: Centerline Pitot-Pressure Trace for a High-Pressure Run

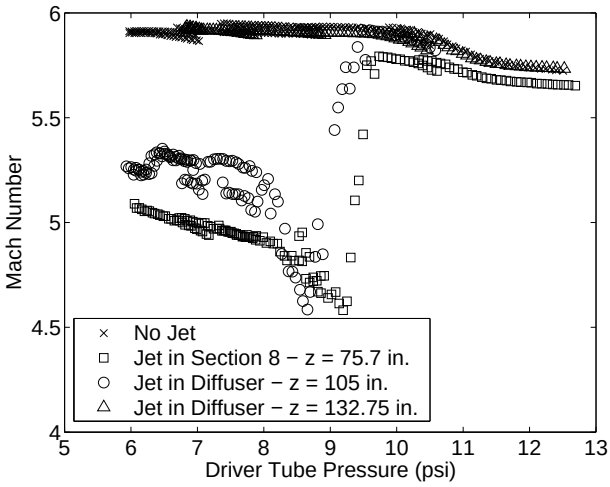

Figure 19: Mach number at $z = 75.3$ inches with a jet in the diffuser

were open for these runs, and the pitot probe was positioned near the nozzle centerline, near $z = 75$ in. The data was acquired using the Tektronix scope at 125kHz and the usual 8 bits per point. The run lasts about 6 sec., and appears similar to runs at lower pressure.

Effect of Downstream Disturbances on Upstream Noise

Adding Controlled Disturbances to the Diffuser

Single jets were introduced into the diffuser at various locations by removing one of the bolts that plug the 1/4-20-in. holes that are used to get static pressure measurements. Since the diffuser drops to near vacuum during the run, the 1 atm air outside the tunnel is allowed to create a jet normal to the wall at a mass flow of about 0.007 kg/s. This mass flow rate was found by allowing the jet to shoot in for about 20 seconds, and calculating the mass flow based on the pressure increase and the volume of the tunnel. Jets in the diffuser were introduced at $z = 75.7, 105.0$, and 132.75 inches. The forward location is in the last section of the nozzle, the middle location is just in front of the sting mount, and the aft location is near the end of the section containing the sting mount.

Fig. 19 shows the Mach number and Fig. 20 shows the RMS pitot fluctuations on the centerline divided by the mean as a function of driver tube pressure; both for a Pitot probe located on the centerline at $z = 75.3$ inches. For the case with no jet, the initial driver tube pressures were 7.98, 7.99, 9.00, 9.99, 10.00, 12.00, and 14.34 psia. For the case with a jet at $z = 75.7$ inches, the initial driver tube pressures were 8.03, 9.02, 10.05, 12.05, and 14.51 psia. For the case with a jet at z=105 inches, the initial driver tube pressures were 7.93, 8.09, 9.13, 10.15, and 12.14 psia. For the case with a jet at z=132.75 inches, the initial driver tube pressures were 8.08, 8.09, 9.02, 10.19, 12.01, and 14.37 psia. The data for the jet at z=132.75 inches and the data with no jet coincide, so the aft jet is too far downstream to affect the Mach number or noise. The middle jet causes separation in the upstream boundary layer at about 9.5 psia, as indicated by the drop in Mach

p_{stag} (psia)	T_0 (deg. R)	p_{pitot} (psia)	M_∞	Re ($\times 10^6$/ft)	RMS Noise (%)
150.7	780	5.444	5.72	3.4	1.4
182.1	780	6.446	5.75	4.1	1.2

Table 2: Initial Runs at High Pressure

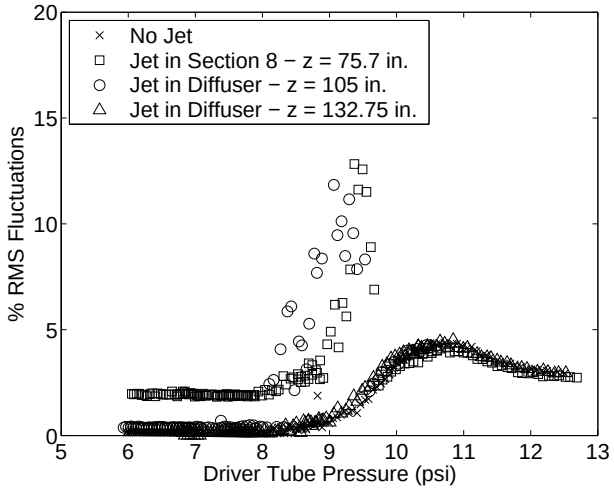

Figure 20: RMS fluctuations at $z = 75.3$ inches with a jet in the diffuser

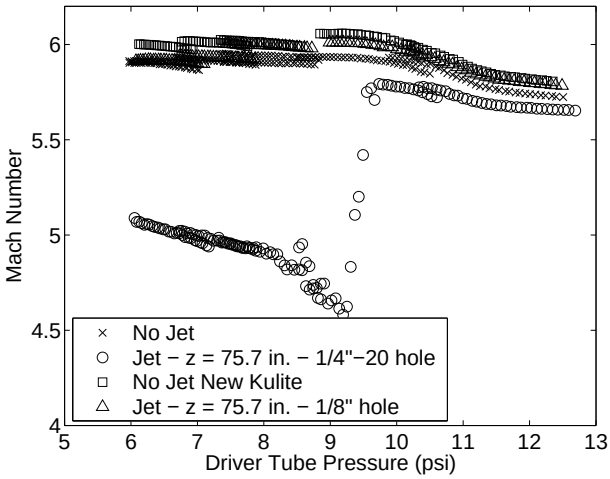

Figure 21: Mach number at $z = 75.3$ in. with a jet at $z = 75.7$ in.

number in Fig. 19. The noise increases at the same point with the unsteady separation but drops down to quiet levels as shown in Fig. 20. The forward jet causes a similar unsteady separation with a large increase in noise. After the separation becomes steady, the noise level does not drop down to quiet levels, but settles at about 2 percent, a remarkable effect that remains to be explained.

Smaller jets were used to find the effect of the size of the jet on the flow quality in the tunnel. The smaller jets were created by drilling holes in 1/4-20-inch bolts and plugging them when not in use. Fig. 21 shows the Mach number on the nozzle centerline for cases with jets of different sizes, as well as a baseline case with no jet with the previous Kulite and the new Kulite. The data taken with the new Kulite has been corrected for the calibration shift due to sensor temperature changes during the run. The 1/4-inch jet had a marked effect, apparently inducing separation at about 9-1/2 psia, while the smaller jet had no measurable effect at this location.

For the case with no jet, the initial driver tube pressures were 7.98, 7.99, 9.00, 9.99, 10.00, 12.00, and 14.34 psia. For the case with a jet at z=75.7 inches through a 1/4-20 inch hole, the initial driver tube pressures were 8.03, 9.02, 10.05, 12.05, and 14.51 psia. For the case with no jet and the new

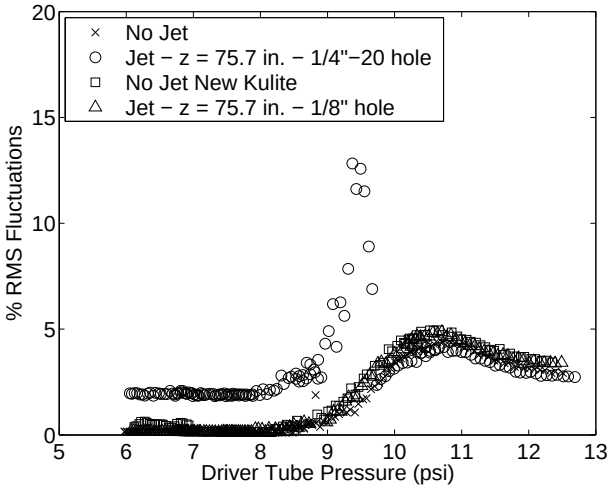

Figure 22: RMS fluctuations at $z = 75.3$ in. with a jet at $z = 75.7$ in.

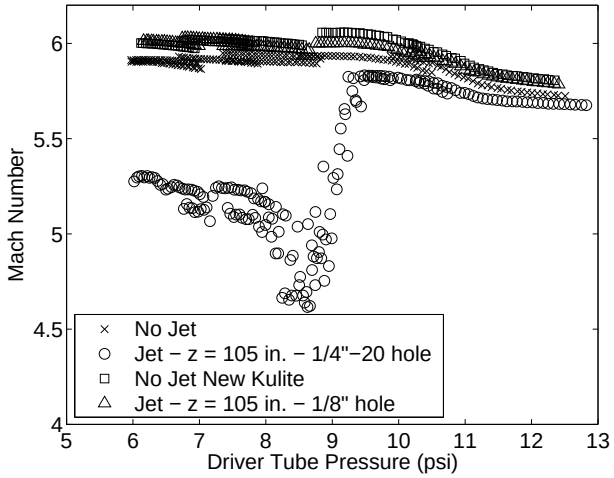

Figure 23: Mach number at $z = 75.3$ in. with a jet in the diffuser at $z = 105$ in.

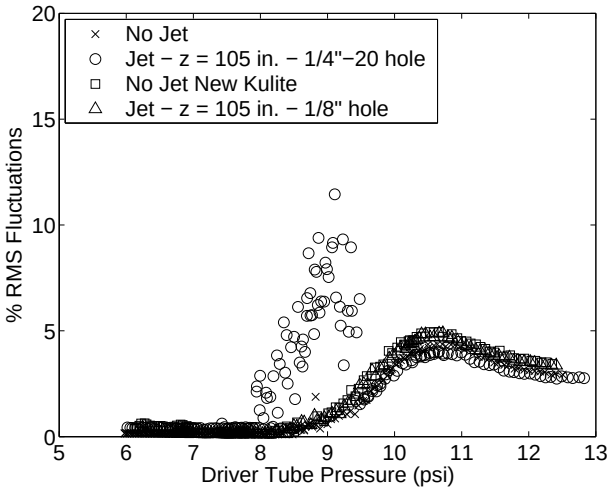

Figure 24: RMS fluctuations at $z = 75.3$ in. with a jet in the diffuser at $z = 105$ in.

Kulite, the initial driver tube pressures were 8.02, 9.03, 10.00, 12.01, and 14.47 psia. For the case with a jet at $z = 75.7$ inches through a 1/8 inch hole, the initial driver tube pressures were 8.03, 9.04, 10.05, 12.05, and 14.45 psia. The case with the jet through a 1/8 inch hole was also measured with the new Kulite. This shows that the new Kulite had an effect on the Mach number that was calculated, which will be discussed in more detail later.

Fig. 22 shows the noise for the same cases. The noise is the same for all cases except for the case with the 1/4-20 inch jet. This shows that the effect of the smaller hole cannot be detected on the centerline at $z = 75.3$ inches. More detailed measurements are needed to determine the limits of the upstream effects of the jets under various conditions.

Fig. 23 and Fig. 24 shows the Mach number and RMS fluctuations for a jet at $z = 105$ inches. The stagnation temperature was $160°C$ and the dewpoint was not measured. For the case with no jet, the initial driver tube pressures were 7.98, 7.99, 9.00, 9.99, 10.00, 12.00, and 14.34 psia. For the case with a jet at $z = 105$ inches through a 1/4-20 inch hole, the initial driver tube pressures were 8.04, 9.08, 10.11, 11.08, 12.08, and14.50 psia. For the case with no jet and the new Kulite, the initial driver tube pressures were 8.02, 9.03, 10.00, 12.01, and 14.47 psia. For the case with a jet at $z = 105$ inches through a 1/8 inch hole, the initial driver tube pressures were 8.06, 9.04, 10.04, 12.00, and 14.46 psia.

The data that was taken with the jets were taken with the new Kulite. This again shows that the smaller jet does not change the flow from the baseline enough to be detected on the centerline at $z = 75.3$ inches. Intermediate sized holes could not be easily examined, since a much larger hole could not be drilled without compromising the structural integrity of the bolt. Modifications will need to be made to the port in the tunnel to allow introducing different jet sizes.

The effect of the azimuthal location of the jet was examined by introducing jets at the same axial location, but different azimuthal locations. The jets were located at $z = 105$ inches, and the Pitot probe was located on the centerline at $z = 75.3$ inches. The azimuthal locations of the jets were at $\phi = 135$ and 315 degrees, where ϕ is measured clockwise from the top, looking downstream. Figs. 25 and 26 show that the separation occurs at nearly the same pressure for either azimuthal location. For the case with the jet at 135 degrees, the initial driver tube pressures were 7.93, 8.09, 9.13, 10.15, and 12.14 psia For the case with the jet at 315 degrees, the initial driver tube pressures were 8.04, 9.08, 10.11, 11.08, 12.08, and 14.50 psia. It is likely that the separation is not axisymmetric and that the location of the jet changes the azimuthal location of the separation, though this could not be determined using a Pitot probe on the tunnel centerline. More detailed measurements are planned to map out this effect.

Temperature Effects on Kulite Calibrations

The Kulites used here are temperature compensated so that a change in temperature of $100°F$ will cause an offset in the calibration that is no more than 1% of full scale. The temperature of the Kulites that

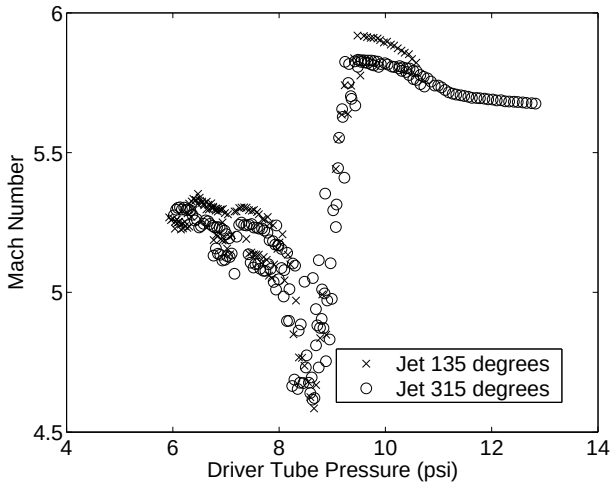

Figure 25: Effect of azimuthal location of jet on Mach number

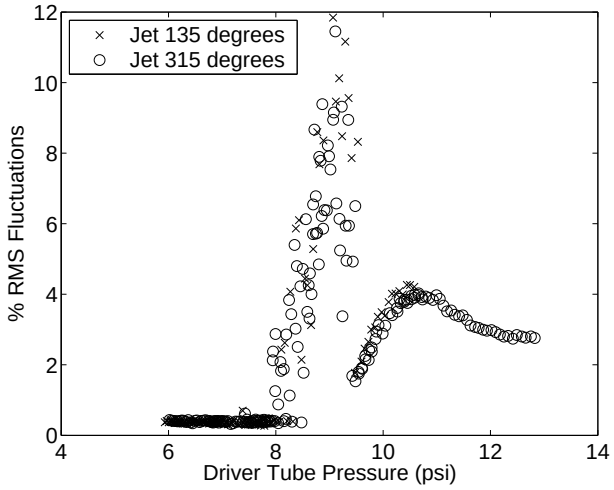

Figure 26: Effect of azimuthal location of jet on noise

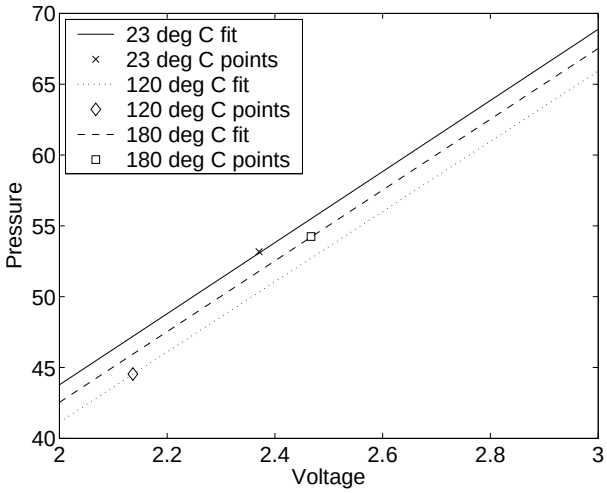

Figure 27: Pressure calibrations with varying temperature

are mounted in the wall of the tunnel is nearly constant since the metal surrounding the sensor has a large thermal inertia. This is why the Kulites must always be calibrated at the temperature that the tunnel is going to be run at.

Fig. 27 shows calibrations carried out for a Kulite mounted at the beginning of the contraction, for varying driver tube temperatures. The full calibrations for the $23°C$, $120°C$ and $180°C$ conditions have 17 points between 0.09 and 152.3 psia, 9 points between 0.04 and 139.4 psia, and 15 points between 0.03 and 149.7 psia, respectively; an expanded view is shown, so the effect of the temperature is visible. The calibration at the middle temperature does not lie between the calibrations at the other temperatures. This does not always occur, but indicates that the calibration shift due to temperature change is not simple or monotonic. For all of the calibrations, the slope stays nearly constant as expected from the Kulite documentation.

The Pitot Kulites are not enclosed in a high thermal-inertia metal, and are heated once the run starts. There is no method at this time to calibrate at a temperature other than near room temperature, and until recently no way to even know how much the temperature of the sensor had changed. However, new stopped Kulites have been obtained. These are the same model number, XCQ-062-15A, but have a fifth wire that can be used to measure the temperature of the sensing resistors on the Kulite diaphragm. Using one of these Kulites, Fig. 28 was generated, showing the temperature change throughout the run at various initial driver

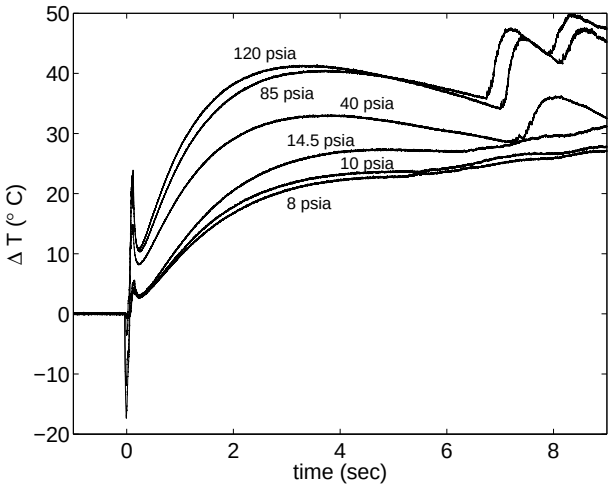

Figure 28: Temperature of Pitot Kulite sensor during run

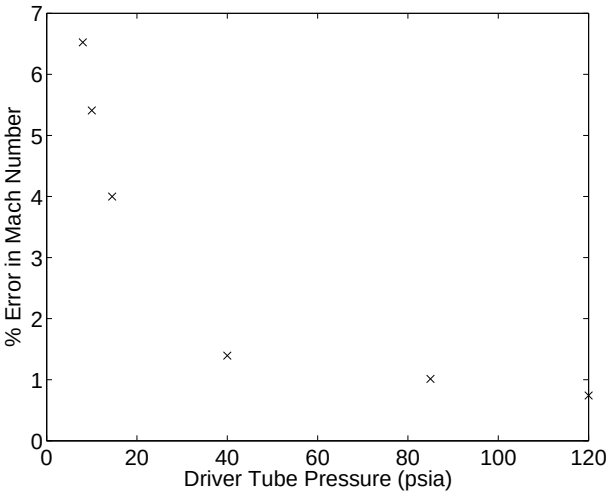

Figure 29: Maximum error in Mach number due to calibration shift

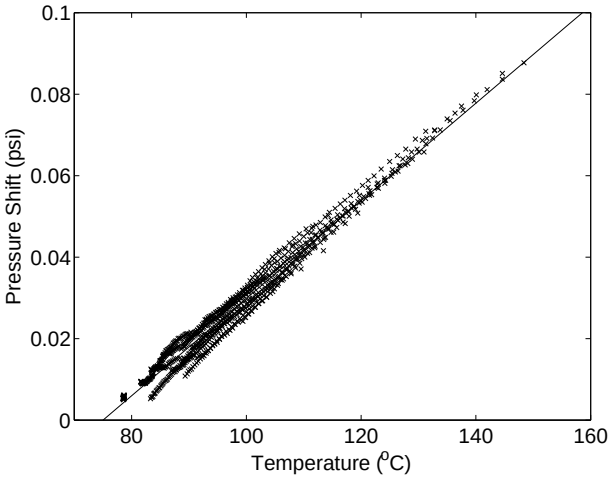

Figure 30: Calibration shift due to temperature change

tube pressures. The initial driver-tube temperature was $160°C$ and sensor starts near room temperature, roughly $25°C$. The temperature of the Kulite does not rise near the stagnation temperature of the driver tube. The diaphragm of the Kulite is behind a small screen, protecting it from damage. This probably allows a pocket of air to insulate the diaphragm from the full stagnation temperature. Using the maximum temperature change, and the Pitot pressure at that time, it was possible to calculate the maximum error in the calculated Mach number, as shown in Fig. 29. This is a large error at the lower pressures; this error could easily account for the shift in Mach number when using a different Kulite.

Since the calibration only shifts during a temperature change, and the fifth wire on the new Kulites can be used to find the temperature of the Kulite, it is possible to compensate for this temperature shift with the new Kulites. The shift was found by heating the Kulite by blowing hot air over it. The air was then shut off and the temperature and voltage from the Kulite were recorded as the Kulite cooled. The tunnel was open, allowing the Kulite to be kept at constant atmospheric pressure. The results from 22 of these records over two days are shown in Fig. 30 with a linear fit through the data. The data was shifted to account for pressure differences between the different sets of data. The calibration shift due to temperature appears to be linear and repeatable.

Fig. 31 shows the effect of correcting for the temperature shift. The data shown was with no disturbances in the driver tube and diffuser and the sting mount empty. These are the same runs shown

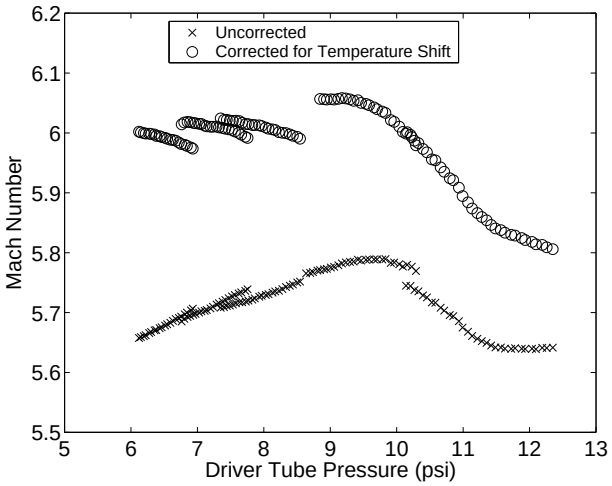

Figure 31: Effect of temperature correction on Mach number

in Fig. 21 and Fig. 23 with no jet and the new Kulite. The effect of the correction is significant. The Mach number now rises as the pressure drops. Although Mach number normally falls as the pressure drops and the boundary-layer thickens, the rise observed here may be caused by the lower pressure boundary-layer becoming laminar farther downstream, and therefore thinner. One might therefore expect that as the pressure drops, the Mach number will first fall due to the thickening turbulent boundary layer, then rise as the boundary layer becomes laminar, and then fall again as the laminar boundary layer thickens. This hypothesis remains to be demonstrated clearly.

Measurements Farther Back in the Nozzle

New measurements performed farther back in the nozzle at $z = 84.3$ inches, with the new streamlined sting support, show a Mach-number drop in nearly every run, presumably due to upstream separation. This seems similar to the separation that was observed farther forward when the double wedge section was earlier in place [13]. Fig. 32 shows the Mach number with respect to driver tube pressure with the new sting mount, without a sting present. The initial driver tube pressures were 6.03, 7.00, 7.97, 8.00, 8.01, 9.02, 10.02, 11.89, and 14.45 psia. This plot shows that there is no correlation between Mach number and driver tube pressure, except that separation does not occur above a driver tube pressure of about 9.5 psia. Fig. 33 shows the noise levels for the same data. This again shows no correlation between noise and driver tube pressure below a pressure of about 9.5 psia. These plots indicate that this

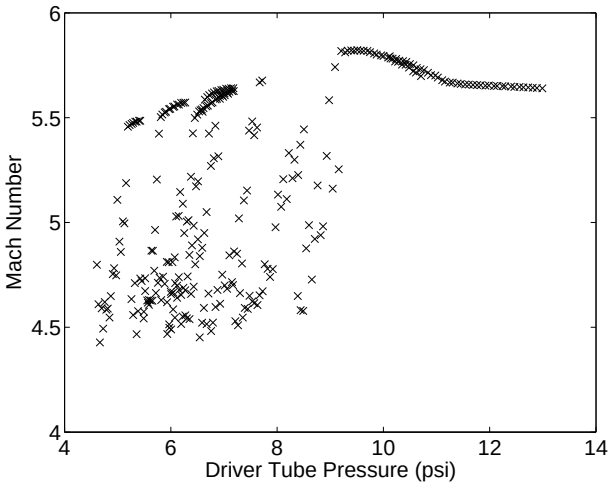

Figure 32: Mach number at $z = 84.3$ inches on the centerline

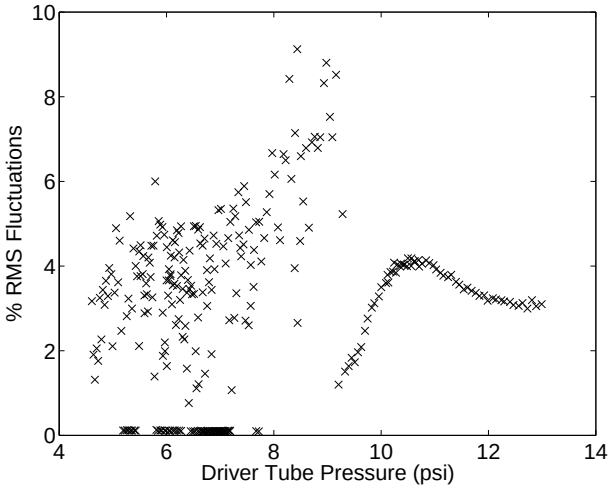

Figure 33: Noise at $z = 84.3$ inches on the centerline

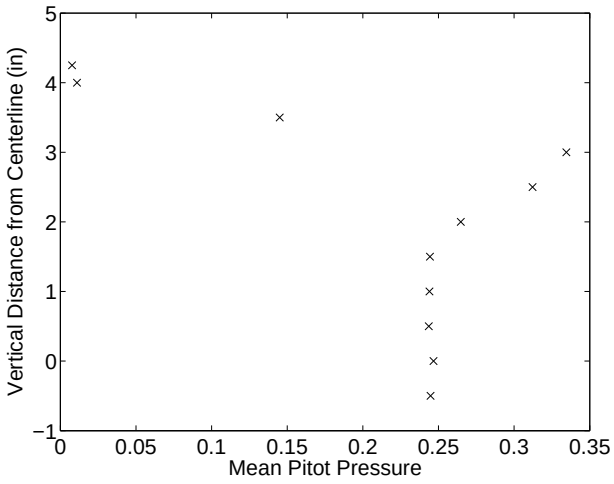

Figure 34: Pressure profile at $z = 75.3$ inches

separation depends on other parameters besides the driver tube pressure. It will probably be necessary to trip the nozzle-wall boundary-layer upstream of the sting support in order to avoid these difficulties with separation.

Quiet-flow Boundary Layer Thickness

A measurement of the pitot pressure profile in the tunnel was obtained while operating with quiet flow, to obtain the laminar boundary layer thickness in the tunnel. This Pitot pressure profile was taken at $z = 75.3$ inches with an initial driver tube pressure of 8 psia $\pm 0.4\%$. The points in the profile shown in Fig. 34 were averaged over a time interval of 2.5 to 2.6 seconds after the start of the run. The driver tube pressure at this time is 7 psia $\pm 0.4\%$ and the driver temperature was $160°C$; the dewpoint was not measured. There appears to be a large overshoot outside the edge of the boundary layer; this could be a result of the operating the nozzle far from the design pressure of 150 psia, or it might conceivably be due to probe interference [19, 20].

In all the cases studied so far, disturbances that are created in a laminar boundary layer cause separation upstream before they trip the upstream flow to turbulence. Thus, at present it appears that downstream disturbances do not cause the early transition on the nozzle wall.

Summary of Quiet-Flow Development Issues

Possible causes of the early transition on the nozzle wall include:

1. Fluctuations generated at the nozzle throat due to problems with the bleed-slot flow. Computations reported in Ref. [15] make this the most likely cause at present.

2. A nozzle-wall temperature distribution that decreases much more rapidly downstream than was initially expected [11]. However, computations suggest this effect should be minor, and there is no evidence to suggest it could cause transition in the way observed.

3. A 0.001-0.002-inch ($Re_k < 12$) rearward-facing step at the downstream end of the electroform [21]. Here, Re_k is a roughness Reynolds number based on the height of the peak roughness, and the conditions in a smooth-wall boundary layer at the roughness height. However, this step was dramatically reduced by the fall 2002 polishing, without noticeable effect [12].

4. Insufficient polish on the downstream nozzle sections (although $Re_k < 12$). However, the fall 2002 polish had no noticeable effect.

5. Fluctuations or nonuniformity in the driver tube flow that lead to early transition. The preliminary measurements carried out to date are only beginning to address this issue; the results so far leave much uncertainty.

6. Some fundamental problem with the use of a very long nozzle which is not captured by the e^N analysis. This seems unlikely, since transition seems to flash forward along the whole downstream half of the nozzle at about the same pressure [14].

7. Noise propagated upstream from the diffuser section. Measurements reported in Ref. [13] show that the original diffuser centerbody caused separation in the nozzle-wall boundary layer when it began to drop laminar. Measurements in the Langley Mach-6 quiet nozzle showed that transition flashed forward on a flared cone when the nozzle exit shock impinged on the aft end of the cone. Upstream propagation of disturbances remained a concern, even with the new model support design, due to the jets of air from the bleed-slot suction that enter the diffuser downstream. However, when jets were removed by plumbing this bleed air directly to the vacuum tank, there was no marked effect [14]. In addition, more recent measurements seem to show that downstream noise sep-

arates an incoming laminar boundary layer before it causes transition.

8. Flaws in the throat-region polish. A small bump can be felt on the bleed lip, and it is possible that this bump is tripping transition. Some small superficial scratches have become visible recently, although the throat remains remarkable clean and free of oil deposits.

9. Leaks in the low-pressure sections that cause jets of air into the nozzle, tripping the boundary layer. Although testing with soap films while the nozzle was under pressure did not show such leaks, small leaks were still a concern. However, the more sensitive leak tests reported here failed to show any leaks in the critical portions of the tunnel (see also Ref. [22]).

10. Vibrations of the bleed lip, introducing disturbances that trip the flow. The tunnel vibrates when the flow starts up, but although these vibrations can clearly be felt, they seem to damp within a second or two. However, the onset of transition seems to occur at the same pressure, regardless of whether this pressure is at the beginning or the end of a run, making this cause seem less likely. The Mach-4 tunnel did not have this problem, but it did not use throat suction either, and the bleed lips may be more sensitive to vibration, particularly in the transverse direction. Measurements of these vibrations are planned.

Progress with the Hot Wire Measurements on Blunt Cones

Calibration in Jet

The hot wire used for the calibration procedure is made of Platinum/10% Rhodium (Pt/Rh), with a diameter of 0.00015 in., a length/diameter ratio of approximately 141, and a cold resistance of 10.5 ohms. The hot wire was connected to an IFA-100 CTA and the first set of runs was completed at a temperature of 290K.

The hot wire was placed in the center of the nozzle exit flow and the chamber pressure was varied from 5 to 90 psia in 5 psi increments. The data was obtained through the use of a LeCroy oscilloscope. The 8-bit oscilloscope was set to take 8 minutes of data per run, sampling at 500 samples/sec. Each run consisted 25 seconds of data at each pressure and allowed for time to change the tunnel pressure between steps and for the pressure to become steady after being increased.

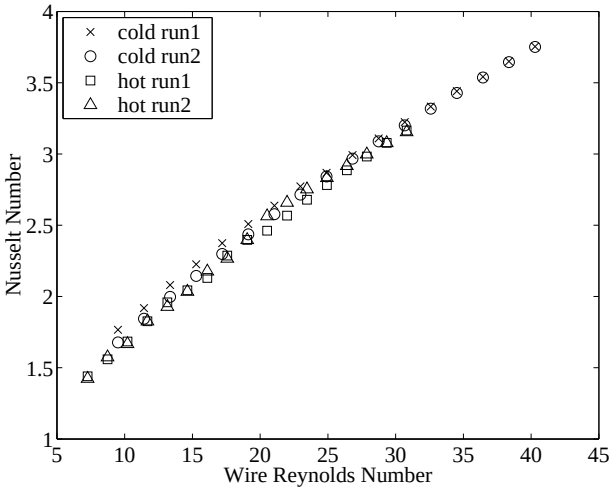

Figure 35: Nusselt number versus wire Reynolds number for four cases in supersonic jet

Fig. 35 shows the Nusselt number plotted against the Reynolds number for the four calibration runs previously described in Ref. [14], obtained at stagnation temperatures of 290K and 360K. The jet Mach number was assumed to be 3.8, based on earlier measurements [23]. The wire Reynolds was calculated using the wire diameter, the mass flux (ρu), and the viscosity based on the stagnation temperature. The data collapse well.

Figs. 36 and 37 show the present data along with data digitized from the plots of Weltmann and Kuhns [24]. The Nusselt vs. Reynolds number data seem to follow a similar pattern, though the Nusselt numbers for a given Reynolds number are approximately 75% larger. This difference could be due to nonuniformities or unsteadiness in the jet flow, end loss effects on the hot wire (which have not yet been taken into account in the present calibration), or other factors. The temperature recovery ratio, η, achieved for a given Knudson number for the two data sets was also compared, as seen in figure 36. The values of η at a given Knudson number are significantly larger for the current data, but again the trends do seem similar with η increasing with an increase in Knudson number. Work continues towards resolving these discrepancies.

Mach-6 Tunnel Runs

Hot wire number F was used for the runs con-

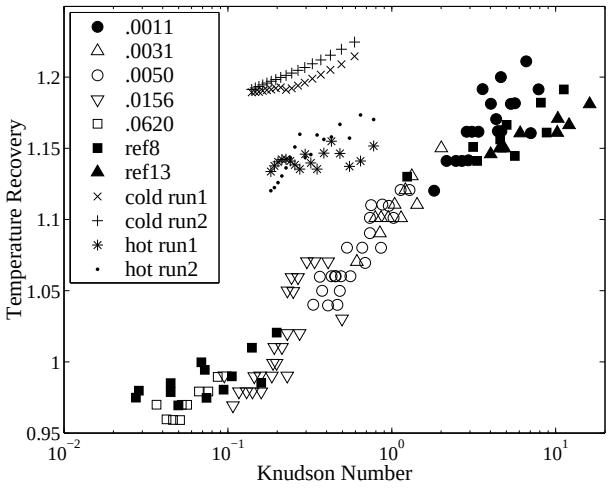

Figure 36: Knudson number versus η comparison with data taken from Weltmann and Kuhns

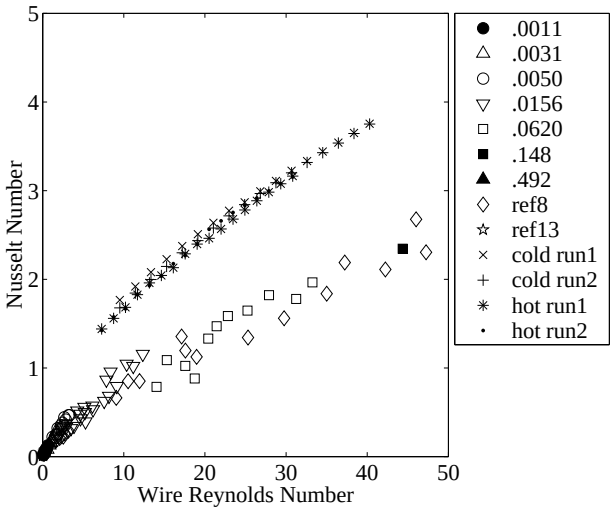

Figure 37: Nusselt vs. Reynolds number comparison with data taken from Weltmann and Kuhns

Figure 38: Hot wire in boundary layer of 7 degree blunt cone

ducted in the Mach-6 tunnel on both the sharp and blunt cones. The cold resistance of the wire was 9.8 ohms, it had a length to diameter ratio of 138 and the overheat ratio was set to approximately 1.8. The square wave frequency response was 240 kHz, as measured in still air at ambient pressures. Fig. 38 shows the hot wire placed near the cone wall.

The sharp cone, which has a 7-deg. half angle, is 16.3 inches in length, and has a base diameter of 4 inches, was placed in the tunnel at a 6-deg. angle of attack. The hot wire was placed 4.8 inches downstream of the nosetip and profiles were obtained on the lee ray for initial driver pressures of 15 and 45 psia and driver pressures of 160°C. For the 15 psia case, the hot wire was originally placed at a height of about 1.5 mm above the wall of the cone. Precise measurements of the hot-wire height await completion of corrective optics allowing use of our short-focus telescope with the curved nozzle window. During the run the hot wire was then traversed outward from the wall in 0.2 mm increments until reaching a height of 5.5 mm. At each step, the hot wire was stationary for 0.1 seconds before moving to the next height, which takes 0.127 seconds. The hot wire was then placed at 5 mm and 7 mm above the cone and the process was repeated in two additional tunnel runs. The data from these runs were combined into one profile (Fig. 39, where z is the axial distance along the cone). The two steps in the mean and rms voltages (at 5 and 7 mm) are due to the different runs being used to complete the plot (and the resulting increase in Reynolds number between the end of one run and the beginning of the next run). It appears from this figure that the edge of the boundary layer is reached somewhere between 6.5 and 7 mm above the cone wall.

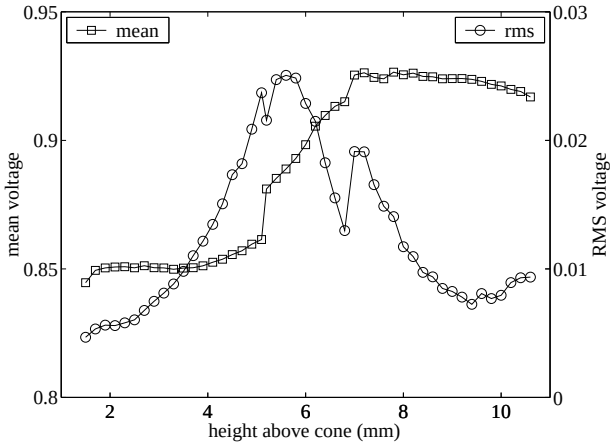

Figure 39: Boundary layer profile of a sharp cone at 6 degree angle of attack, 15 psia, and $z = 4.8$ inches

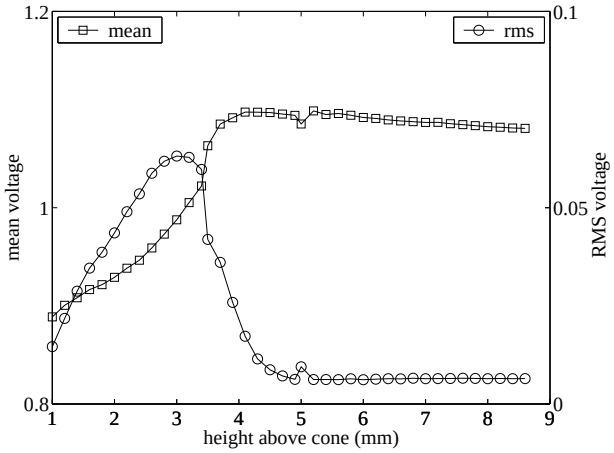

Figure 40: Boundary layer profile of a sharp cone at 6 degree angle of attack, 45 psia, and $z = 4.8$ inches

A similar set of runs were conducted at an initial driver pressure of 45 psia with the hot wire placed at heights of 1, 3.5, and 5 mm above the cone wall and are illustrated in Fig. 40. The boundary layer thickness for this pressure is approximately 3.5 mm; the thickness is roughly half at the three-times higher pressure, near what would be expected from a simple laminar boundary-layer scaling.

The blunt cone also has a 7-deg half angle and is 22.25 inches long with a base diameter of 5.5 inches. The nosetip radius is 0.020 inches. The cone was placed in the tunnel at zero angle of attack and measurements were taken at 4 different axial locations (12, 14, 16, and 18 inches aft of the nosetip) to illustrate the growth of the boundary layer (Fig. 41). The thickness of the boundary layer can be

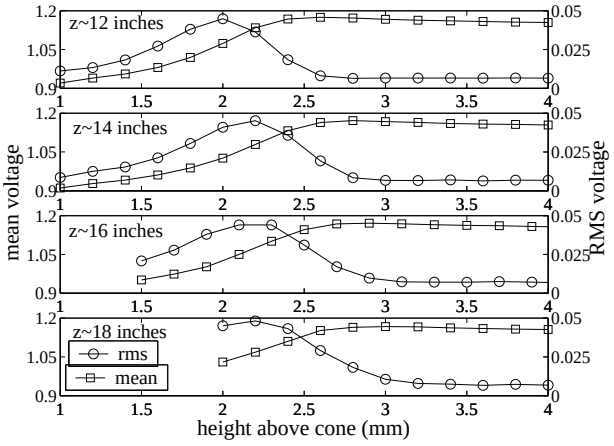

Figure 41: Boundary layer profile on a 7 degree cone at zero angle of attack and 45 psia

seen to grow from approximately 2.4 to 2.7 mm. A peak in the rms voltage is seen, in each of the runs, near the edge of the boundary layer. The boundary layer thickness increases downstream, and the fluctuations peak near the boundary-layer edge, both as expected. The boundary layers are thinner at zero angle of attack, as expected, despite the fact that the measurements were obtained much further downstream. Future plans include quantitative comparisons to Navier-Stokes computations.

Summary

Purdue University continues to develop the 9.5-inch Mach-6 Boeing/AFOSR Mach-6 Quiet Tunnel. The tunnel is being modified to run at higher pressures, with presumably conventional noise, to study transition and the transition mechanisms for blunt cones at angle of attack. Preliminary hot-wire measurements on the lee side of cones at angle of attack show boundary-layer thicknesses that are much larger than at zero angle of attack, as expected. The main focus of the work remains the search for high Reynolds number quiet flow. Although related computations suggest that a small separation bubble on the bleed lip is the mostly likely cause of the early transition presently observed, measurements in the contraction entrance continue, showing small fluctuations especially near the wall. Continuing measurements of the fluctuations downstream of the nozzle suggest that such disturbances will separate an upstream laminar boundary layer before they cause it to trip.

Acknowledgements

The research is funded by AFOSR under grant F49620-03-1-0030, and by Sandia National Laboratory under contract 80377. Frank Chen and Steve Wilkinson from NASA Langley continued to provide occasional assistance in making the best possible use of information available from the earlier NASA Langley quiet-tunnel development effort.

REFERENCES

[1] John Croft. Weapons delivery goes hypersonic. *Aerospace America*, pages 38–42, May 2004.

[2] Steven P. Schneider. Hypersonic laminar-turbulent transition on circular cones and scramjet forebodies. *Progress in Aerospace Sciences*, 40(1-2):1–50, 2004.

[3] I.E. Beckwith and C.G. Miller III. Aerothermodynamics and transition in high-speed wind tunnels at NASA Langley. *Annual Review of Fluid Mechanics*, 22:419–439, 1990.

[4] Steven P. Schneider. Effects of high-speed tunnel noise on laminar-turbulent transition. *Journal of Spacecraft and Rockets*, 38(3):323–333, May–June 2001.

[5] Steven P. Schneider. Flight data for boundary-layer transition at hypersonic and supersonic speeds. *Journal of Spacecraft and Rockets*, 36(1):8–20, 1999.

[6] S. P. Wilkinson, S. G. Anders, and F.-J. Chen. Status of Langley quiet flow facility developments. Paper 94-2498, AIAA, June 1994.

[7] I. Beckwith, T. Creel, F. Chen, and J. Kendall. Freestream noise and transition measurements on a cone in a Mach-3.5 pilot low-disturbance tunnel. Technical Paper 2180, NASA, September 1983.

[8] Alan E. Blanchard, Jason T. Lachowicz, and Stephen P. Wilkinson. NASA Langley Mach 6 quiet wind-tunnel performance. *AIAA Journal*, 35(1):23–28, January 1997.

[9] S. P. Schneider and C. E. Haven. Quiet-flow Ludwieg tube for high-speed transition research. *AIAA Journal*, 33(4):688–693, April 1995.

[10] Steven P. Schneider. Design of a Mach-6 quiet-flow wind-tunnel nozzle using the e**N method for transition estimation. Paper 98-0547, AIAA, January 1998.

[11] Steven P. Schneider, Shin Matsumura, Shann Rufer, Craig Skoch, and Erick Swanson. Progress in the operation of the Boeing/AFOSR Mach-6 quiet tunnel. Paper 2002-3033, AIAA, June 2002.

[12] Steven P. Schneider, Shin Matsumura, Shann Rufer, Craig Skoch, and Erick Swanson. Hypersonic stability and transition experiments on blunt cones and a generic scramjet forebody. Paper 2003-1130, AIAA, January 2003.

[13] Steven P. Schneider, Craig Skoch, Shann Rufer, and Erick Swanson. Hypersonic transition research in the Boeing/AFOSR Mach-6 quiet tunnel. Paper 2003-3450, AIAA, June 2003.

[14] Steven P. Schneider, Craig Skoch, Shann Rufer, Erick Swanson, and Matt Borg. Bypass transition on the nozzle wall of the Boeing/AFOSR Mach-6 quiet tunnel. Paper 2004-0250, AIAA, January 2004.

[15] Ezgi S. Taskinoglu, Doyle D. Knight, and Steven P. Schneider. A numerical analysis for the bleed slot design of the Purdue Mach-6 wind tunnel. Paper 2005-XXXX, AIAA, January 2005. Submitted to the Aerospace Sciences Meeting.

[16] T. Vrebalovich. On supersonic wind tunnels with low free-stream disturbances. *J. Applied Mechanics*, 27:362–364, June 1960.

[17] J.M. Kendall, Jr. Experimental study of cylinder and sphere wakes at a Mach number of 3.7. Technical Report 32-363, NASA Jet Propulsion Laboratory, November 1962.

[18] Steven P. Schneider, Shann Rufer, Laura Randall, and Craig Skoch. Shakedown of the Purdue Mach-6 quiet-flow Ludwieg tube. Paper 2001-0457, AIAA, January 2001.

[19] M. V. Morkovin and W.S. Bradfield. Probe interference in measurements in supersonic laminar boundary layers. *Journal of the Aeronautical Sciences*, 21(11):785–787, November 1954.

[20] James M. Kendall, Jr. An experimental investigation of leading-edge shock-wave–boundary-layer interaction at Mach 5.8. *J. Aero. Sci.*, 24:47–56, January 1957.

[21] Steven P. Schneider and Craig Skoch. Mean flow and noise measurements in the Purdue Mach-6 quiet-flow Ludwieg tube. Paper 2001-2778, AIAA, June 2001.

[22] Craig Skoch. Leak testing. Informal lab report in draft form, dated 5 April 2004. 6 pages.

[23] Phillip M. Schneider. Flow measurements in a Mach 4 axisymmetric jet. Purdue University, School of Aeronautics and Astronautics. A 29 page laboratory report with 11 figures, May 1999.

[24] Ruth N. Weltmann and Perry W. Kuhns. Heat transfer to cylinders in crossflow in hypersonic rarefied gas streams. Technical Note TN-D-267, NASA, March 1960.